STGlow: A Flow-based Generative Framework with Dual Graphormer for Pedestrian Trajectory Prediction

Rongqin Liang, Student Member, IEEE, Yuanman Li, Member, IEEE, Jiantao Zhou, Senior Member, IEEE, and Xia Li, Member, IEEE

Abstract—Pedestrian trajectory prediction task is an essential component of intelligent systems, and its applications include but are not limited to autonomous driving, robot navigation, and anomaly detection of monitoring systems. Due to the diversity of motion behaviors and the complex social interactions among pedestrians, accurately forecasting the future trajectory of pedestrians is challenging. Existing approaches commonly adopt GANs or CVAEs to generate diverse trajectories. However, GAN-based methods do not directly model data in a latent space, which makes them fail to have full support over the underlying data distribution; CVAE-based methods optimize a lower bound on the log-likelihood of observations, causing the learned distribution to deviate from the underlying distribution. The above limitations make existing approaches often generate highly biased or unnatural trajectories. In this paper, we propose a novel generative flow based framework with dual graphormer for pedestrian trajectory prediction (STGlow). Different from previous approaches, our method can more accurately model the underlying data distribution by optimizing the exact loglikelihood of motion behaviors. Besides, our method has clear physical meanings to simulate the evolution of human motion behaviors, where the forward process of the flow gradually degrades the complex motion behavior into a simple behavior, while its reverse process represents the evolution of a simple behavior to the complex motion behavior. Further, we introduce a dual graphormer combining with the graph structure to more adequately model the temporal dependencies and the mutual spatial interactions. Experimental results on several benchmarks demonstrate that our method achieves much better performance compared to previous state-of-the-art approaches.

Index Terms—Generative flow, trajectory prediction, graph learning, attention mechanism, deep neural network.

I. Introduction

Trajectory prediction, as one of the most important future behavior modeling tasks, aims to predict the future trajectory based on the observed trajectory. It plays an important role in applications such as self-driving vehicles [1], autonomous navigation robots [2], anomaly behavior detection [3], [4], video surveillance [5]–[7] and so on.

Despite that significant advances have been achieved recently [8]–[15], predicting future trajectories of pedestrians accurately remains challenging due to the inherent properties of pedestrians. First, due to the differences of human intent and

unique behavior patterns, the future trajectories of pedestrians are full of diversity, even when they share the same historical trajectory. Second, influenced by surrounding agents, there are highly complex social interactions among pedestrians, which drive pedestrians to make decisions such as walking parallel, walking in groups, or changing direction / speed to avoid collisions. Faced with the challenge of diverse future trajectories, most previous works [8], [11]-[14], [16] applied generative models to model the multi-modality of human motion behaviors. For instance, to predict plausible and diverse trajectories, some works [8], [11], [13] employed generative adversarial networks (GANs) [17] to predict the distribution of future trajectories. Nevertheless, GAN-based methods do not directly model data in a latent space, which may make them fail to have full support over the underlying data distribution, thus generating highly biased trajectories. In addition, the training process of GANs is often unstable due to the adversarial learning. Alternatively, some works exploited conditional variational auto-encoders (CVAEs) [16], [18]–[21] or diffusion model [14] to model the diversity of future trajectories. However, both of them optimize a lower bound on the log-likelihood of observations, which may cause the learned distribution to deviate from the underlying distribution and the generated future trajectories are unnatural. To straightforwardly model the social interactions among pedestrians, some works [9], [22]–[24] proposed to represent the social interactions between pedestrians utilizing the topology of graphs. However, these graph-based methods suffer from over-smoothing problems on node features, which means that when constructing the graphs for crowded environments, the features of nodes will be smoothed by the aggregation of lots of nodes, thus may lead to the loss of unique behavior characteristics of pedestrians.

Faced with the above challenges on diverse trajectories and social interactions, in this paper, we propose a novel flow-based generative framework with dual graphormer for pedestrian trajectory prediction (STGlow). For the diversity of trajectories, we propose a generative flow framework with pattern normalization (Glow-PN) to produce multiple plausible trajectories. Similar to the process of artists creating artworks, complex motion behaviors of pedestrians are not accomplished at one stroke, but based on simple motion behaviors (e.g., every step of walking or every action) combined with individual behavior habits originating from various 'biases' such as people's walking habits, traffic awareness, and potential intentions. Hence, we propose to characterize the evolution

R. Liang, Y. Li and X. Li are with School of Electronics and Information Engineering, Shenzhen University, Shenzhen, China. (Corresponding author: Yuanman Li, email: yuanmanli@szu.edu.cn.)

J. Zhou is with the State Key Laboratory of Internet of Things for Smart City, and also with the Department of Computer and Information Science, University of Macau. e-mail: jtzhou@um.edu.mo.

of motion behavior from simple to complex by modeling the 'biases' progressively utilizing the generative flow with a series of simple and tractable functions. Besides, we propose a dual graphormer combining with the graph structure to extract the representations of motion behaviors and model the temporal dependencies and the mutual spatial interactions. Specifically, in the training phase, a Glow-PN is applied to learn the distribution of the motion behavior conditioned on the representation of social interactions. In the inference phase, simple behaviors are sampled from the standard normal distribution and formed into "evolved" representations of complex motion behaviors using the reverse process of Glow-PN conditioned on the representation of social interactions. These representations of complex motion behaviors are eventually decoded into predicted trajectories through a bidirectional trajectory prediction module. The main contributions of our work can be summarized as follows:

- We present a novel diverse trajectory prediction framework based on generative flow, simulating the evolution of human motion behaviors from simple to complex. In contrast to previous approaches, our method can more accurately model the underlying distribution by optimizing the exact log-likelihood of motion behaviors. Besides, a pattern normalization is carefully developed to normalize the unique behavior pattern of pedestrians, greatly improving the prediction accuracy.
- 2) We further propose a dual graphormer to extract the representations of motion behaviors and model the social interactions in both temporal and spatial domains. Different from previous Transformer based methods, our dual graphormer combined with the graph structure more adequately models the temporal dependencies and the mutual spatial interactions.
- 3) The proposed framework achieves state-of-the-art performance on widely used pedestrians trajectory prediction benchmarks, providing a promising direction for generating diverse and natural trajectories.

The remainder of this paper is organized as follows. Section III gives a brief review of related work. Section III details our proposed STGlow for pedestrian trajectory prediction. Extensive experimental results are presented in Section IV, and we finally draw a conclusion in Section V.

II. RELATED WORKS

A. Pedestrian Trajectory Prediction

Traditional trajectory prediction methods mainly rely on designing handcrafted rules to model human interactions [25]–[29]. For instance, Social Force [25] introduced attractive and repulsive forces to avoid collisions. Although these methods demonstrate the importance of interaction modeling, they are limited by the handcrafted features and perform poorly in trajectory prediction.

Recently, with the great success of deep neural networks, the Recurrent Neural Network (RNN) and its variants are widely applied in trajectory prediction tasks [1], [30]–[32], on the basis of their good performance on sequence learning [33]–[35]. Wherein, Social-LSTM [30] employed a Long Short-

Term Memory (LSTM) to encode pedestrian trajectory and designed a Social Pooling to aggregate the global representation of neighboring pedestrians. To enhance the representation ability of social interaction features, many studies [1], [32], [36], [37] have followed this idea of transmitting information between pedestrians and proposed different effective message passing mechanisms. Although the RNN-based approaches approach the trajectory prediction task in a data-driven manner, they ignore the important fact that the future trajectories of pedestrians are full of diversity due to the differences of human intents and unique behavior patterns.

2

Besides, the graph networks are employed to model the complex social interactions among pedestrians due to their intuitive modeling power of non-euclidean structure data [9], [22], [23], [38]–[40]. For instance, the work GTPPO [23] explored a social graph attention module that combines specific obstacle avoidance experiences (OAEs) with the graph attention to capture pedestrians' social interactions. DMRGCN [40] proposed a disentangled multi-scale aggregation to better represent social interactions between pedestrians on a weighted graph. Though the topology of graphs seems to be a straightforward way to represent social interactions, graph-based methods suffer from over-smoothing problems on node features [40], [41], which may lead to the loss of the unique behavior characteristics of pedestrians.

To generate diverse future trajectories, some researchers suggested employing generative models to model the diversity of human motion behaviors [8], [42], [43]. Part of these works were based on GANs [8], [11], [13]. Among them, Social-GAN [8] applied GANs for the first time to generate diverse future trajectories and designed a pooling module to aggregate social interactions. Furthermore, TPNMS [11] proposed a temporal pyramid structure to model both global and local contexts of human motion behaviors. Another part of the works [12], [16], [18], [20], [21] applied CVAEs to explicitly encode the distribution of diverse future trajectories. For instance, Trajectron++ [16] utilized the latent variable framework of CVAEs to explicitly encode diversity and modeled social interactions in combination with a graph-structured recurrent model, while PECNet [18] embedded the distant trajectory endpoints into a latent space to assist in long-range diverse trajectory prediction. More recently, MID [14] devised a Transformer-based diffusion model for trajectory prediction with a reverse process of motion indeterminacy diffusion. Though previous generative models have achieved promising performance in modeling the diversity of human behaviors, these approaches still have inherent limitations, e.g., methods based on GANs may not fully support the data distribution due to the lack of encoding latent variables, while methods based on CVAEs and diffusion models optimize a lower bound on the log-likelihood of observations. Such limitations could make them generate biased or unnatural trajectories.

B. Normalizing Flow

Normalizing Flows (NFs) are invertible generative models that map complex data distributions to simple and tractable ones. Recently, NFs have been successfully applied to a variety

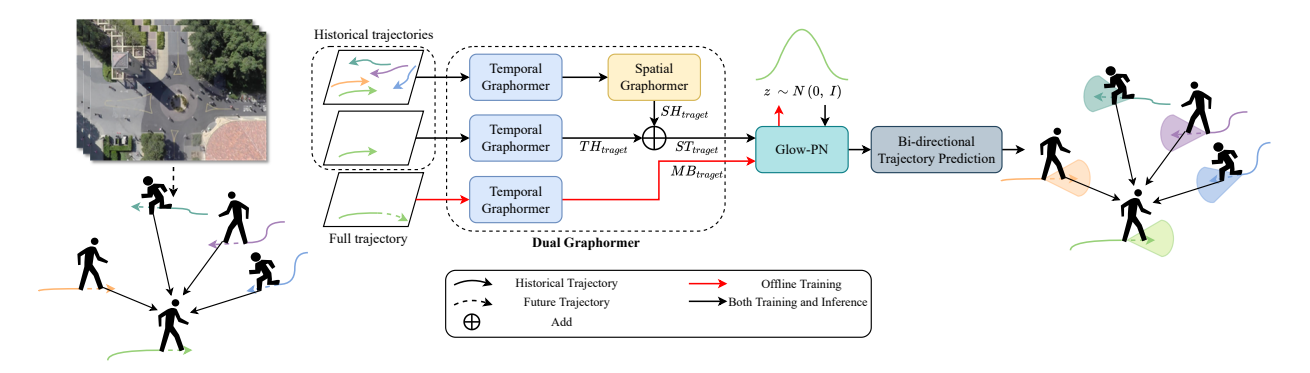


Fig. 1. The framework of our STGlow algorithm. STGlow primarily consists of a dual graphormer, a generative flow with pattern normalization (Glow-PN) and a bi-directional trajectory prediction module. 1) First, the full trajectory of the target pedestrian is encoded into the representation of complex motion behavior through the temporal graphormer, while the historical trajectories are encoded into the representation of social interaction through the temporal and spatial graphormer; 2) then, a Glow-PN is applied to learn the distribution of complex motion behaviors using a series of simple reversible transformation, conditioned on the social interactions; 3) simple behaviors sampled from the standard normal distribution evolve into complex motion behaviors through the reverse process of Glow-PN, which are eventually fed into the bi-directional trajectory prediction module to predict diverse future trajectories.

of generation tasks such as image generation [44]–[47], video generation [48], speech synthesis [49], [50]. For example, Glow [46] proposed an invertible 1×1 convolution for the generative flow and showed the efficiency of realistic-looking synthesis and manipulation of large images. WaveGlow [49] proposed a flow-based network for generating high-quality speech from mel-spectrograms. In our task, we propose a flow-based method for pedestrian trajectory prediction. Our proposed scheme has clear physical meanings to simulate the evolution of human motion behaviors.

C. Transformer

Transformer [51], which relies entirely on self-attention mechanisms to model global dependencies of the serialization inputs, has recently made remarkable progress in a variety of natural language processing (NLP) tasks [52], [53], vision tasks [54]–[57] and speech recognition [58]. For instance, in vision tasks, ViT [54] sequentialized the image into a series of tokens and modeled the global dependencies of the image through the Transformer encoder. More recently, some works [10], [12], [14] have applied Transformer to pedestrian trajectory prediction tasks. Among them, STAR [10] employed a temporal transformer and spatial transformer respectively to extract temporal dependencies and spatial interactions, while AgentFormer [12] exploited an agent-aware Transformer to learn representations from both temporal and spatial dimensions. Different from prior works, in this work, we devise a dual graphormer, which can more adequately model the temporal dependencies and the mutual spatial interactions.

III. PROPOSED APPROACH: STGLOW

The overall framework of STGlow model is illustrated in Fig. 1. It primarily consists of three components: 1) a dual graphormer to extract the representations of motion behaviors and model the temporal dependencies and the mutual spatial interactions; 2) a generative flow with pattern normalization (Glow-PN) to learn the underlying distribution of complex motion behaviors, conditioned on the social interactions; 3) a bi-directional trajectory prediction module to forecast diverse future trajectories.

A. Problem Formulation

Given N pedestrians with observed trajectories $\mathcal{X}=\{X_1^{(-t_o+1:0)},...,X_N^{(-t_o+1:0)}\}$ from time steps T_{-t_o+1} to T_0 in the scene, the trajectory prediction algorithm aims to predict the future trajectories $\mathcal{Y}=\{Y_1^{(1:t_p)},...,Y_N^{(1:t_p)}\}$ of all pedestrians in the upcoming time steps T_1 to T_{t_p} , where $X_i^t=(x_i^t,y_i^t)\in\mathbb{R}^2$ is the position of the i-th pedestrian at the time step t. The trajectory prediction algorithm takes as input the observed trajectories with t_o time steps of all pedestrians in a scene, and aims to predict their future trajectories in the next t_p time steps by a model $f(\cdot)$, denoted by

$$\hat{\mathcal{Y}} = f(\mathcal{X}; W^*), \tag{1}$$

where $\hat{\mathcal{Y}}$ is the set of future trajectories predicted by $f(\cdot)$ and W^* represents the set of learnable parameters in the model.

For the sake of brevity, we hereafter drop the superscript when there is no ambiguity, *i.e.*, $X_i \triangleq X_i^{(-t_o+1:0)}$ and $Y_i \triangleq Y_i^{(1:t_p)}$. We further use X,Y to represent a generic history trajectory and the corresponding future trajectory, respectively.

B. Dual Graphormer

Influenced by surrounding agents, pedestrians have highly complex social interactions while walking, which may enforce pedestrians to make decisions such as walking parallel, walking in groups, or changing direction / speed to avoid collisions. Obviously, such social interactions contain both temporal dependencies and spatial interactions, which are fundamentally important for accurately predicting trajectories. In this work, we design a dual graphormer to more adequately model the temporal dependencies and the mutual spatial interactions. As shown in Fig. 1, our dual graphormer primarily consists of two components: 1) a temporal graphormer, and 2) a spatial graphormer.

1) Temporal Graphormer: In this work, we decouple temporal dependencies into the behavior-independent temporal dependencies and behavior-dependent temporal dependencies. The former type of dependencies reveals the importance of each previous time step to the future trajectory. The other

Fig. 2. Illustration of the temporal graphormer.

type of dependencies models the relationships among different previous motion behaviors across the temporal domain.

Assume that there are T time steps of each trajectory, denoted by $X_i^{1:T}$. The temporal graphormer takes $X_i^{1:T}$ as input and outputs a set of embeddings $TH_i^{1:T}$ with temporal dependencies, which we define as **Temporal Embedding**. Specifically, we first construct a temporal graph

$$G_{tmp} = (V_{tmp}, A_{tmp}), (2)$$

by treating each time step as a node of the graph. Here $V_{tmp} = \{V_t | t=1,...,T\}$ represents nodes of G_{tmp} . A_{tmp} is the adjacency matrix describing the temporal dependencies, i.e., the motion behavior at a given time can only be affected by previous motion states rather than future motion states. Based on this fact, we define A_{tmp} as

$$A_{tmp}^{ij} = \begin{cases} 1, & i \ge j \\ -inf, & i < j \end{cases}, i, j \in [1, T].$$
 (3)

To model the behavior-independent temporal dependencies, we design a centrality encoding that learns a centrality embedding based on the length of the *influence duration* of each time step, which is formulated as

$$C_i^t = Linear\left(Deg\left(V_t\right), \Theta_C\right); t \in [1, T], \tag{4}$$

where $C_i^t \in \mathbb{R}^D$, Θ_C is the set of learnable parameters, and $Deg(V_t)$ calculates the outdegree of the node V_t . The centrality encoding adaptively explores the importance of different time steps based on the influence duration.

For behavior-dependent temporal dependencies, we first adopt a non-linear multi-layer perceptron (MLP) to embed the position X_i^t at each time step as

$$H_i^t = MLP\left(X_i^t, \Theta_N\right),\tag{5}$$

where Θ_N contains the learnable parameters, and $H_i^t \in \mathbb{R}^D$. Besides, a positional embedding $P_i^t \in \mathbb{R}^D$ is applied to label the position of the motion state at each time step in a trajectory. In this paper, we encode the time step positions in a learnable way, as proposed in [59]. Then, we update the node embedding by

$$H_i^t := H_i^t + C_i^t + P_i^t. (6)$$

According to the Transformer encoder [51], we further map H_i into three values

$$Q_i = H_i^{1:T} W_O, \ K_i = H_i^{1:T} W_K, \ V_i = H_i^{1:T} W_V,$$
 (7)

where W_Q , W_K , W_V are the parameters corresponding to the Query Q_i , Key K_i and Value V_i of the pedestrian i. The output of temporal graphormer can be further computed as

$$Att\left(Q_{i},K_{i},V_{i}\right) = Softmax\left(\frac{Q_{i}\left(K_{i}\right)^{T}}{\sqrt{d_{k}}}\odot A_{tmp}\right)V_{i}, \quad (8)$$

where A_{tmp} is the adjacency matrix, \odot is the operation of dot product, and d_k is the dimension of Q_i . Eq. (8) characterizes the behavior-dependent temporal dependencies, which builds the relationships among different motion behaviors across the temporal domain. For brevity, we write the temporal graphormer as

$$TH_i^{1:T} = TG\left(X_i^{1:T}; \Theta_{tq}\right),\tag{9}$$

where $TH_i^{1:T}$ is the *Temporal Embedding* of the temporal graphormer, and Θ_{tg} contains learnable parameters. By resorting to the temporal graphormer, both the behavior-independent temporal dependencies and behavior-dependent temporal dependencies can be characterized.

2) Spatial Graphormer: The information of relative positions to other pedestrians is crucial for a target pedestrian to make decisions, such as adjusting velocity or direction to avoid collisions. However, considering only the relative positions to the neighbors is not sufficient for making a reasonable decision. For example, when a neighbor in the rear is walking toward the opposite direction from the target pedestrian, the target pedestrian generally does not need to make adjustments, despite their close proximity. In reality, the relative steering angle of a neighbor to the target pedestrian and the walking direction of the target pedestrian are also the key elements to drive the pedestrians to make changes of the motion states.

To fully model the mutual spatial interactions between pedestrians, in this work, we propose a spatial graphormer by utilizing the relative motion states of the neighbors (*i.e.*, the relative position and the relative steering angle to the target pedestrian) and the walking direction of the target pedestrian.

Specifically, we take the pedestrians in the scene as nodes and construct an undirected graph based on the walking direction of the target pedestrian and the relative motion states of the neighbors. First, at the time step t, we can construct the spatial graph as

$$G_{spa} = (V_{spa}, A_{spa}), \tag{10}$$

where V_{spa} represents the nodes of G_{spa} , and A_{spa} is the adjacency matrix of G_{spa} describing the mutual spatial relation-

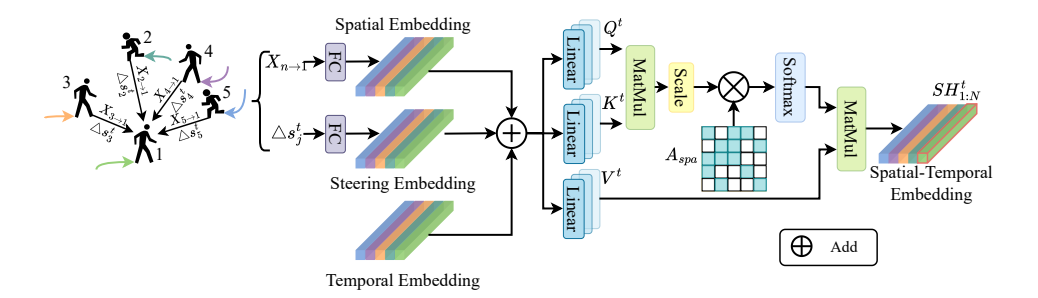


Fig. 3. Illustration of the spatial graphormer.

ships among pedestrians. To better capture spatial interactions, we endow each node $V_i^t \in V_{spa}$ with the information of both relative positions and relative steering angles. Namely,

$$V_i^t = R_i^t + S_i^t + TH_i^t, (11)$$

where TH_i^t represents the temporal embedding of the pedestrian i at the time step t, R_i^t and S_i^t represent the embedding of the relative position and the relative steering angle of the pedestrian i to the target pedestrian, respectively. As shown in Fig. 3, we adopt a single layer MLP with ReLU activation to embed the relative position and relative steering angle of neighbors as

$$R_j^t = MLP\left(x_{j\to i}^t, y_{j\to i}^t; \Theta_P\right),$$

$$x_{j\to i}^t = x_j^t - x_i^t; \ y_{j\to i}^t = y_j^t - y_i^t,$$
(12)

$$S_{j}^{t} = MLP(\Delta s_{j}^{t}; \Theta_{S}),$$

$$\Delta s_{j}^{t} = \frac{\Delta X_{i}^{t} \cdot \Delta X_{j}^{t}}{|\Delta X_{i}^{t}||\Delta X_{j}^{t}|},$$
(13)

where $(x_{j \to i}^t, y_{j \to i}^t)$ is the relative position of the neighbor j to the target pedestrian i at the time step t, $\triangle s_j^t$ represents the corresponding relative steering angle, $\triangle X_i^t = (\triangle v x_i^t, \triangle v y_i^t) = (x_i^t - x_i^{t-1}, y_i^t - y_i^{t-1})$ denotes the walking direction of the pedestrian i at the time step t, and Θ_P , Θ_S are the parameters of MLP. We refer to R_j^t as the spatial embedding, and S_j^t as the steering embedding. Note that we do not employ positional encoding when modeling spatial interactions since there is no natural order for pedestrians in the scene.

Intuitively, people commonly pay little attention to the pedestrians out of their view. For simplicity, we set the maximum binocular field of view to 180° in the horizontal position for a pedestrian. Based on this fact, we design the adjacency matrix A_{spa} as

$$A_{spa}^{ij} = \begin{cases} 1, & if \ x_{j \to i}^t \cdot \triangle v x_i^t \ge 0 \ and \ y_{j \to i}^t \cdot \triangle v y_i^t \ge 0, \\ -inf, & Otherwise, \end{cases}$$
(14)

where $(\triangle v x_i^t, \triangle v y_i^t)$ is the walking direction of the pedestrian i along x and y axes, and $(x_{j \to i}^t, y_{j \to i}^t)$ is the relative position of the neighbor j to the pedestrian i. A_{spa}^{ij} characterizes the mutual spatial relationships among pedestrians.

Similar to the temporal graphormer, the output of the spatial graphormer can be further computed as,

$$Q^{t} = SH_{1:N}^{t}W_{Q'}, \quad K^{t} = SH_{1:N}^{t}W_{K'}, \quad V^{t} = SH_{1:N}^{t}W_{V'},$$
$$Att\left(Q^{t}, K^{t}, V^{t}\right) = Softmax\left(\frac{Q^{t}\left(K^{t}\right)^{T}}{\sqrt{d_{k}}} \odot A_{spa}\right)V^{t},$$

$$(15)$$

where N is the number of pedestrians in the scene, $W_{Q^{\prime}},W_{K^{\prime}},W_{V^{\prime}}$ are the parameters. For brevity, we write the spatial graphormer as

$$SH_{1:N}^t = SG\left(X_{1:N}^{t-1:t}, TH_{1:N}^t; \Theta_{sh}\right),$$
 (16)

where $SH_{1:N}^t$ is the output of the spatial graphormer, which we define as **Spatial-Temporal Embedding**. Θ_{sh} is the set of parameters. Similar to [51], the multi-head attention mechanism is employed in our framework. Note that different from graph-based methods, our dual graphormer takes the advantage of the self-attention mechanism to avoid direct aggregation of connected nodes, which could greatly alleviate the oversmoothing problem. Such a conclusion has been carefully justified in [41].

3) Proposed Dual Graphormer in Trajectory Prediction: In order to model the behavior pattern of pedestrians, we first apply the Dual Graphormer to extract the deep representations of *motion behaviors* and *social interactions*. As shown in Fig. 1, we primarily extract representations of two types of inputs, *i.e.*, the full trajectory and the observed historical trajectory. Note that the full trajectories are used only in the training phase.

The full trajectory reflects the motion behavior of each pedestrian in a time period, such as where to go and how to go. In our STGlow model, we define the representation of the full trajectory as the *motion behavior* of each pedestrian, which can be formulated as

$$MB_{target} = TG\left(Concat\left(X_{target}, Y_{target}\right), \Theta_{tg}\right), \quad (17)$$

where $TG(\cdot)$ is the temporal graphormer.

Besides, the observed historical trajectories of all pedestrians in the scene are encoded via the temporal and spatial graphormer to extract the *social interactions* of the target pedestrian, which can be written as

$$TH_{1:N} = TG(X_{1:N}; \Theta_{tgh}),$$

$$SH_{target} = SG(X_{1:N}^{-1:0}, TH_{1:N}^{0}; \Theta_{sgh}),$$

$$TH_{target} = TG(X_{target}; \Theta_{tgy}),$$

$$ST_{target} = TH_{target} + SH_{target}.$$
(18)

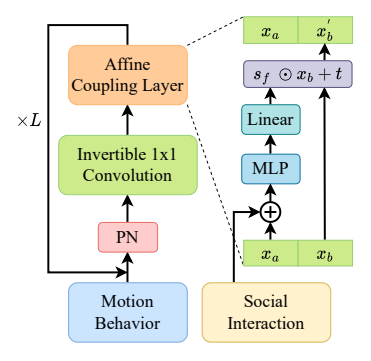


Fig. 4. Illustration of the proposed generative flow with Pattern Normalization (Glow-PN).

where Θ_{tgh} , Θ_{sgh} and Θ_{tgy} are parameters. So far, we have obtained the representation MB_{target} of **motion behavior** of the target pedestrian and the mutual **social interaction** ST_{target} . In the inference phase, we first predict the latent motion behavior MB_{target} conditioned on the ST_{target} . The MB_{target} is then fed into a decoder to generate future trajectories.

C. Proposed Generative Flow with Pattern Normalization (Glow-PN)

Due to the differences of human intent and unique behavior patterns, the motion behaviors of pedestrians are of high diversity. Namely, the future trajectories could be very different given the same historical trajectory. Thus, learning the underlying distribution of motion behaviors conditioned on social interactions is important to predict the diverse trajectories of pedestrians. Existing approaches commonly use GANs or CVAEs to generate diverse trajectories, where their limitations have been carefully discussed in the first section.

In our work, we simulate the process of degradation and evolution between the complex motion behavior and a simple behavior as follows:

$$MB_{target} \stackrel{f_1}{\longleftrightarrow} h_1 \stackrel{f_2}{\longleftrightarrow} h_2 \cdots \stackrel{f_k}{\longleftrightarrow} z,$$
 (19)

where $\{f_1, f_2, ..., f_k\}$ denote a set of *invertible* transformations to simulate the degrading and evolving process, and $h_1, ..., h_{k-1}$ denote the intermediate motion behaviors. We can see that the forward process of formula (19) gradually degrades the complex motion behavior MB_{target} into a simple behavior z, while its reverse process represents the evolution of a simple behavior to the complex motion behavior.

In reality, the complex motion behavior MB_{target} of pedestrians is not accomplished at one stroke, but based on simple motion behaviors z (e.g., every step of walking or every action) combined with individual behavior habits which may originate from various aspects such as people's walking habits, traffic awareness, and potential intentions. For the sake of simplicity, we assume that z follows a standard normal distribution, i.e.,

$$z \sim \mathcal{N}\left(z; 0, I\right),\tag{20}$$

where I is an identity matrix. Letting $x \triangleq MB_{target}$, the log-likelihood of complex motion behavior can be written as:

$$\log p_{\theta}(x) = \log \left(p_{\theta}(z) \left| \det \left(\frac{dz}{dx} \right) \right| \right) \tag{21}$$

$$= \log p_{\theta}(z) + \sum_{i=1}^{K} \log \det (dh_i/dh_{i-1}) | \quad (22)$$

$$= \log p_{\theta}(z) + \sum_{i=1}^{K} \log \det \left(J\left(f_{i}^{-1}(x)\right) \right) |. \quad (23)$$

The equation (21) holds because $\int_x p_\theta(x) \, dx = \int_z p_\theta(z) \, dz$, and the equation (23) holds because $h_i = f_i^{-1}(h_{i-1})$. The first term in formula (23) is the log-likelihood of the standard normal distribution and the scalar value $\log |\det \left(J\left(f_i^{-1}(x)\right)\right)|$ is the logarithm of the absolute value of the determinant of the Jacobian matrix $J\left(f_i^{-1}(x)\right)$. This value reflects the transformation from h_{i-1} to h_i of the motion behavior under the transformation f_i . Then, our framework optimizes the parameters by minimizing the negative log-likelihood function, where the loss is

$$L_p = \min -\sum_{i=1}^{N} \log p_{\theta}(x_i).$$
 (24)

In contrast to previous approaches, our method can more accurately model the underlying data distribution by optimizing the exact log-likelihood of motion behaviors as shown in (24). Obviously, how to design the invertible transformation functions $f_1, ..., f_k$ is essential for the optimization of (24). We should bear in mind that $f_1, ..., f_k$ should be differentiable thus allowing the end-to-end training.

In our work, we employ Glow [46] to learn the invertible transformations of motion behaviors from complex to simple. As shown in Fig. 4, for the forward process, we take *motion behavior* MB_{target} as input of Glow-PN. After several "steps of flow", the complex *motion behavior* is degraded into a simple behavior that can be represented by a simple distribution. A step of flow here consists of a pattern normalization (PN), an invertible 1×1 convolution, and an affine coupling layer, described below.

1) Pattern Normalization (PN): Considering the fact that diverse motion behaviors share the same behavior pattern (e.g., the individual walking habits), we propose a pattern normalization (PN) for trajectory prediction as shown in Fig. 5. Different from the Actnorm adopted in the original Glow, PN performs normalization for multiple motion behaviors jointly at the sample axis. As will be shown in the experiments, our proposed PN greatly improves the prediction performance.

Specifically, the forward function, reverse function and logdeterminant of our proposed PN are calculated as:

Function:
$$y = s_g \odot x + b$$
,
Reverse Function: $x = (y - b)/s_g$, (25)
Log determinant: $\log |s_g|$,

where x indicates the input of PN, and y signifies its output. Both x and y are tensors of shape $(K \times C \times 1)$ with K motion behaviors and channel dimension C. $s_g, b \in \mathbb{R}^{K \times C}$ are learnable scales and bias parameters whose initialization





Fig. 5. In ActNorm, (H, W) as the size of the feature map and C as the channel axis, while in PN, K as the sample axis and C as the feature axis. N as the batch axis. The pixels in blue are normalized by the same learnable scales and bias.

depends on the input data, so that the data has zero mean and unit variance after PN. After initialization, the scale and bias are treated as regular trainable parameters that are independent of the data. Note that, different from Layer Normalization [60], to ensure that the transformation f is invertible, we design the forward and reverse process of normalization in PN. The forward process normalizes the behavior pattern of each pedestrian to promote model convergence, while the reverse process de-normalizes multiple motion behaviors to restore its original motion characteristics.

2) Invertible 1×1 Convolution: In order that all channels of input in the forward transformation can be updated in subsequent coupling layers, we following Glow apply an invertible 1×1 convolution layer before coupling layers. The weights W of convolution are initialized as a random rotation matrix and hence invertible. Thus, the log-determinant of this transformation is easy to compute:

$$f_{conv}^{-1} = Wy, (26)$$

$$f_{conv}^{-1} = Wy,$$

$$\log |\det \left(J\left(f_{conv}^{-1}(y)\right)\right)| = \log |\det (W)|,$$
(26)

where the log-determinant starts at zero and after one SGD step, the values start to diverge from zero.

3) Affine Coupling Layer: Generally, computing the determinants of high-dimensional Jacobian and large matrices is very expensive. Following Glow, we reduce the complexity by designing tractable and flexible invertible transformation. Specifically, we introduce an affine coupling layer, which can efficiently compute forward function, reverse function and logdeterminant.

$$x_a, x_b = split\left(x_{affine}\right),\tag{28}$$

$$\left(\log s_f,t\right) = Linear\left(MLP\left(concat\left(x_a,ST_{target}\right)\right)\right), \ \ (29)$$

$$x_{b}^{'} = s_{f} \odot x_{b} + t, \tag{30}$$

$$x' = concat\left(x_a, x_b'\right),$$
 (31)

where $x_{affine} \in \mathbb{R}^{1 \times C \times K}$ represents the input of affine coupling layer, the $split(\cdot)$ function splits x into two havles along the channel dimension, while the $concat(\cdot)$ operation performs the restore operation. Since the inputs x_a of formula (29) remains unchanged during the affine transformation operation, formula (29) can be arbitrary transformation. Accordingly, in the reverse process of the affine coupling layer, s_f and t can be obtained from the output x_a through formula (29), and x_b can be obtained by the reverse of x_b . Note that our affine coupling layer is conditioned on the social interaction ST_{target} to establish the mapping of complex to simple motion behaviors.

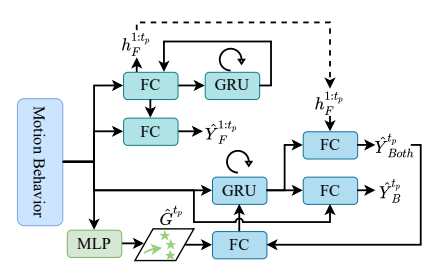


Fig. 6. Illustration of the bi-directional trajectory prediction module.

As we can see, only the s_f term changes the volume of the mapping in the affine coupling layer and adds a change of variables term to the loss. The log-determinant of the affine coupling layer and the final likelihood are hence computed as follows:

$$\log |\det \left(J\left(f_{coupling}^{-1}\left(x\right)\right)\right)| = \log |s_f|. \tag{32}$$

$$\log p_{\theta}(x) = \log p_{\theta}(z) + \sum_{j=0}^{n} \left(\log |s_g^j| + \log \det |W^j| + \log |s_f^j| \right),$$
(33)

where $p_{\theta}\left(z\right) = \mathcal{N}\left(z;0,I\right)$, and its log-likelihood can be easily computed as: $-z\left(x\right)^{T}z\left(x\right)/2\sigma^{2}$, where $\sigma=I$. So far, we have eventually completed the design of the invertible transformation of "step of flow". Note that, different from the CVAE-based methods, our method optimizes the exact loglikelihood of motion behaviors.

D. Bi-directional Trajectory Prediction

Due to the invertible design of Glow-PN, a simple behavior drawn from the standard normal distribution can be directly evolved into a complex motion behavior MB_{target} through the reverse process of Glow-PN, conditioned on the social interaction ST_{target} . Then, we feed the obtained MB_{target} into the decoder to predict the future trajectory.

1) Bi-directional Decoder with Goal Estimation: To alleviate the error accumulation issue caused by the recurrent neural network in trajectory prediction, as shown in Fig. 6, we adopt the decoder proposed in Bitrap [20], which is designed in a bi-directional manner. We additionally predict and supervise the forward and backward future trajectory to strengthen the representation learning during bidirectional prediction. Specifically, we first predict the goal of each pedestrian as

$$\hat{G}^{t_p} = MLP\left(MB'_{target}; \Theta_g\right), \tag{34}$$

where MB'_{target} is the representation of complex motion behaviors evolved by the reverse process of Glow-PN from simple behaviors. Then, the forward trajectory \hat{Y}_F^t is predicted

$$f_{i}^{t-1} = MLP\left(f_{h}^{t-1}; \Theta_{fi}\right),$$

$$f_{h}^{t} = GRU\left(f_{h}^{t-1}, f_{i}^{t-1}; \Theta_{ff}\right),$$

$$\hat{Y}_{F}^{t} = FC\left(concat\left(f_{i}^{t}, MB_{target}'\right); \Theta_{fy}\right),$$
(35)

where t from 1 to t_p represents the time step of the forward prediction, and $f_h^0 = MLP\left(MB_{target}^{'}; \Theta_{fh}\right)$. Further, the backward prediction $\hat{Y}_B^{t_b}$ is formulated as

$$b_{h}^{t_{b}} = GRU\left(b_{i}^{t_{b}+1}, b_{h}^{t_{b}+1}; \Theta_{bh}\right),$$

$$\hat{Y}_{B}^{t_{b}} = FC\left(concat\left(b_{h}^{t_{b}}, MB_{target}'\right); \Theta_{by}\right),$$
(36)

where t_b from t_p-1 to 1 represents the time step of the backward prediction, and $b_h^{t_p} = MLP\left(MB_{target}';\Theta_{bh}\right)$. Last, the bidirectional prediction $\hat{Y}_{Both}^{t_b}$ considering both forward and backward trajectories is predicted as

$$\hat{Y}_{Both}^{t_b} = FC\left(concat\left(b_h^{t_b}, f_i^{t_b}\right); \Theta_{both}\right),
b_i^{t_b} = MLP\left(\hat{Y}_{Both}^{t_b}, \Theta_{bi}\right),$$
(37)

where $b_i^{t_p} = MLP\left(\hat{G}^{t_p}, \Theta_{bi}\right)$. Besides, Θ_* indicates the set of parameters. We supervise the predicted forward, backward and bidirectional trajectories as

$$L_{traj} = \min_{k \in K} \alpha \|G_k^{t_p} - \hat{G}_k^{t_p}\| + \min_{k \in K} \sum_{t=1}^{t_p} (\lambda_1 \|Y_k^t - \hat{Y}_F^t\| + \lambda_2 \|Y_k^t - \hat{Y}_B^t\| + \lambda_3 \|Y_k^t - \hat{Y}_{Both}^t\|),$$
(38)

where K represents the number of samples of future trajectories, and α , λ_1 , λ_2 , λ_3 are the coefficients that balance different losses. Combined with the log-likelihood of the motion behaviors, our final loss is formulated as

$$L_{total} = L_p + \sum_{i=1}^{N} L_{traj}.$$
 (39)

2) Inference: In the inference phase, we can easily generate the diverse trajectories by simple behaviors sampled from the standard normal distribution through the reverse process of Glow-PN conditioned on social interactions.

IV. EXPERIMENTS

In this section, we evaluate the performance of our proposed STGlow, which is implemented using the PyTorch framework. All the experiments are performed on Ubuntu 18.04 with an NVIDIA 3090 GPU. Our source code and trained models will be publicly available upon acceptance.

A. Implementation Details

The dimension of the node embedding is set as 256, and the number of coupling layers and invertible 1×1 convolutions are empirically set as 16. We also output 64 of the channels after every 4 coupling layers. In the training phase, the number of samples of predicted trajectories is set to 20 and the coefficients of the final loss are set to be 1, 0.25, 0.25, 0.5, respectively. We adopt Adam algorithm [62] to optimize the loss function (39) and train our network with the following hyper-parameter settings: batch size is 128; learning rate is 1e-3; betas are 0.9 and 0.999; weight decay is 1e-6 and the number of epochs is 400.

B. Datasets and Metrics

Datasets: We evaluate our method on two benchmark public pedestrian trajectory prediction benchmarks including ETH/UCY dataset [29], [63] and Stanford Drone Dataset (SDD) [64]. The ETH and UCY dataset group consists of 5 video sequences: ETH & HOTEL (from ETH) and UNIV, ZARA1, & ZARA2 (from UCY). All trajectories are converted to world coordinates, so the results we report are in meters. SDD comprise of more than 11000 unique pedestrians across 20 top-down scenes captured on the stanford university campus in bird's eye view containing several moving agents like humans and vehicles. We use the standard test train split as used in [18] and other previous works.

Metrics: For the sake of fairness, we adopt the evaluation metrics Average Displacement Error (ADE) and Final Displacement Error (FDE) which are commonly used in literature [8], [9], [12], [30]. ADE computes the average $\ell 2$ distance between the predictions and the ground truth future while FDE computes the $\ell 2$ distance between the predicted and ground truth at the last observed point. The number of observed time steps is 8 (3.2 seconds) of each person and the upcoming trajectory of 12 time steps (4.8 seconds) is used to predict. For the ETH/UCY dataset, we use the widely adopted leave-one-out approach evaluation methodology such that we train our model on four scenes and test on the remaining one [8], [11], [13]. Considering the diversity of future trajectories, we use the Best-of-K strategy to compute the final ADE and FDE with K=20.

C. Baselines

We compare with the following baselines including previous state-of-the-art methods: *GAN-based methods:* S-GAN [8], TPNMS [11], TPNSTA [13]. *CVAE-based methods:* Trajectron++ [16], AgentFormer [12], PECNet [18], BiTraP [20]. *Graph-based methods:* Social-STGCNN [9], SGCN [22], DMRGCN [40], GTPPO [23]. *Transformer-based methods:* AgentFormer [12], STAR [10]. *Other methods:* Y-Net [19], CAGN [61], SIT [65], MID [14].

D. Quantitative Analysis

We quantitatively compare our *STGlow* with a wide range of current methods. Table I provides the comparison between our method and existing algorithms on the ETH/UCY dataset. Besides the performance on each dataset, we report the average results for each method in the last two columns. Noted that, we also report the sampling number since adding the sampling number can effectively promote the performance. Based on the results, we draw the following conclusions:

- In general, with the same sampling number, our method STGlow outperforms all the previous approaches in terms of ADE and FDE of all datasets.
- Compared with the GAN-based [8], [11], [13] method, our method achieves significant performance gains on ADE and FDE metrics. For example, Our method achieves 59% and 61% relative improvements in average ADE and FDE metrics over the GAN-based method

Datasets	Sampling	ETH		Hotel		Univ		Zara1		Zara2		AVG	
Methods		ADE	FDE	ADE	FDE	ADE	FDE	ADE	FDE	ADE	FDE	ADE	FDE
S-GAN [8]	20	0.87	1.62	0.67	1.37	0.76	1.52	0.35	0.68	0.42	0.84	0.61	1.21
Social-STGCNN [9]	20	0.64	1.11	0.49	0.85	0.44	0.79	0.34	0.53	0.30	0.48	0.44	0.75
GTPPO [23]	20	0.63	0.98	0.19	0.30	0.35	0.60	0.20	0.32	0.18	0.31	0.31	0.50
TPNMS [11]	20	0.52	0.89	0.22	0.39	0.55	1.13	0.35	0.70	0.27	0.56	0.38	0.73
TPNSTA [13]	20	0.51	0.87	0.22	0.39	0.52	1.09	0.34	0.68	0.26	0.54	0.37	0.71
STAR [10]	20	0.56	1.11	0.26	0.50	0.52	1.15	0.41	0.90	0.31	0.71	0.41	0.87
Trajectron++ [16]	20	0.39	0.83	0.12	0.21	0.20	0.44	0.15	0.33	0.11	0.25	0.19	0.41
AgentFormer [12]	20	0.45	0.75	0.14	0.22	0.25	0.45	0.18	0.30	0.14	0.24	0.23	0.39
PECNet [18]	20	0.54	0.87	0.18	0.24	0.35	0.60	0.22	0.39	0.17	0.30	0.29	0.48
SGCN [22]	20	0.63	1.03	0.32	0.55	0.37	0.70	0.29	0.53	0.25	0.45	0.37	0.65
DMRGCN [40]	20	0.60	1.09	0.21	0.30	0.35	0.63	0.29	0.47	0.25	0.41	0.34	0.58
Y-Net+TTST [19]	<u>10000</u>	0.28	<u>0.33</u>	0.10	0.14	0.24	0.41	0.17	0.27	0.13	0.22	0.18	0.27
CAGN [61]	20	0.41	0.65	0.13	0.23	0.32	0.54	0.21	0.38	0.16	0.33	0.25	0.43
MID [14]	20	0.39	0.66	0.13	0.22	0.22	0.45	0.17	0.30	0.13	0.27	0.21	0.38
BiTraP [20]	20	0.37	0.69	0.12	0.21	0.17	0.37	0.13	0.29	0.10	0.21	0.18	0.35

TABLE I QUANTITATIVE RESULTS ON THE ETH/UCY DATASET WITH BEST-OF-20 STRATEGY IN ADE/FDE METRIC. LOWER IS BETTER.

TABLE II

QUANTITATIVE RESULTS ON THE SDD DATASET WITH BEST-OF-20

STRATEGY IN ADE/FDE METRIC. * MEANS THE RESULTS ARE
REPRODUCED BY [14] WITH THE OFFICIAL RELEASED CODE. LOWER IS
BETTER.

20

0.31

0.49

0.09

0.14

0.16

0.33

0.12

0.24

STGlow (ours)

Methods	Sampling	ADE	FDE	
S-GAN [8]	20	27.23	41.44	
PECNet [18]	20	9.96	15.88	
Y-Net + TTST [19]	10000	7.85	11.85	
Y-Net* [19]	20	8.97	14.61	
GTPPO [23]	20	10.13	15.35	
Trajectron++* [16]	20	8.98	19.02	
SIT [65]	20	8.59	15.27	
MID [14]	20	7.61	14.30	
STGlow (ours)	20	7.20	11.20	

TPNSTA. In addition, compared with the methods based on CVAEs [12], [16], [18], [20] and diffusion model [14], our method also achieves a greater performance improvement due to the optimization of the exact log-likelihood of motion behavior rather than the variational lower bound. For instance, our method improves the average ADE and FDE metrics by 17% and 20% respectively compared with the best CVAE-based method BiTraP [20], and 29% and 26% respectively compared with MID [14].

• Compared with the graph-based approach [9], [22], [23], [40] that models social interactions in an intuitive way, we integrate the graph structure with the Transformer structure in modeling social interactions and achieve significant performance improvements. For example, compared with DMRGCN [40], our STGlow improves 56% and

52% in average ADE and FDE metrics respectively.

0.09

0.19

0.15

0.28

We can draw similar conclusions above on SDD, as shown in Table II, which indicates that the proposed STGlow method has better generalization performance. It is worth noting that STGlow achieved a relative improvement of 20% and 23% in ADE and FDE metrics compared to Y-Net [19] without using 'TTST' post-processing. Furthermore, compared with the current state-of-the-art MID [14] method, our method achieves the best performance on ADE and FDE metrics.

E. Qualitative Analysis

In this subsection, we visualize some examples to further illustrate the ability of our STGlow to fully exploit complex social interactions between pedestrians and generate plausible, natural and diverse future trajectories.

1) Results in different scenarios: As can be drawn from Table I, the methods based on CVAEs perform significantly better than the methods based on GANs. Thus, we qualitatively compare the most-likely predictions between STGlow and the previous state-of-the-art CVAE-based method, BiTraP [20], on all five scenes of the ETH/UCY dataset.

Overall, as shown in Fig. 7, our prediction results are significantly closer to the ground truth trajectory compared with BiTraP, regardless of simple scenarios or scenarios with complex interactions. Specifically, the first row illustrates simple motion behaviors in five scenarios, including uniform walking and simple interactions. In these scenarios, the trajectories predicted by our method are significantly closer to the ground truth trajectories, since we more accurately model the underlying distribution by optimizing the exact log-likelihood of motion behaviors. The second and third rows show more complex motion behaviors, including slowing down, speeding

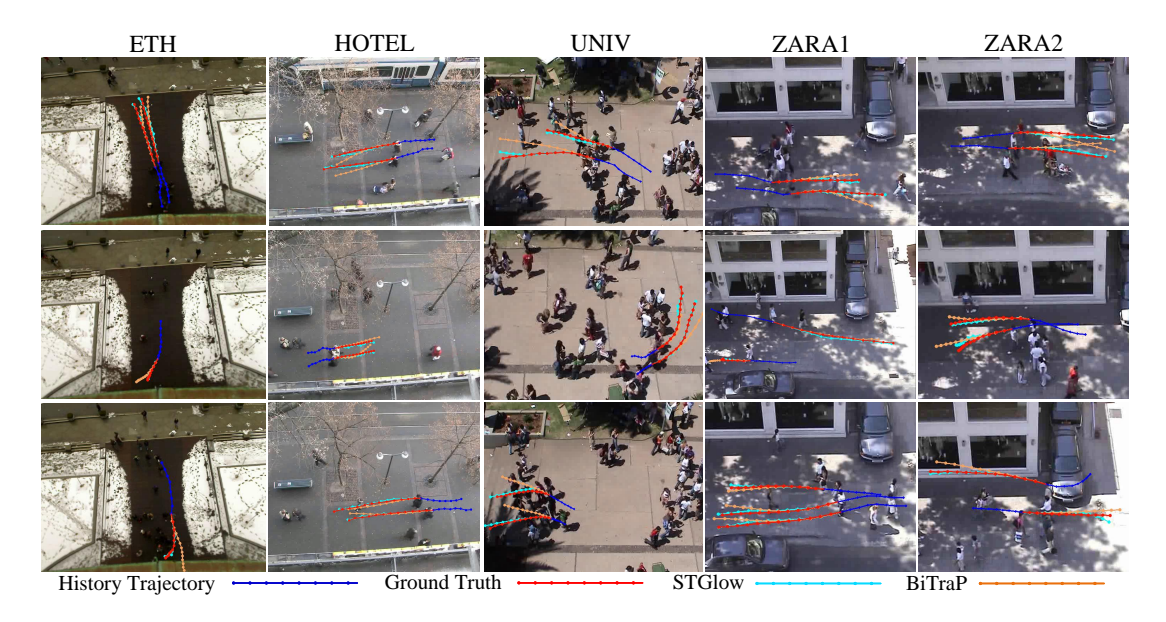


Fig. 7. Visualization of predicted trajectories on the ETH/UCY Dataset. Given the history trajectories (blue line), we illustrate the ground truth paths (red line) and predicted future trajectories by our STGlow (green line) and the previous state-of-the-art BiTrap (orange line) for five different scenes, and dots are the locations of pedestrians at different time steps. Best viewed in color and zoom-in for more clarity.

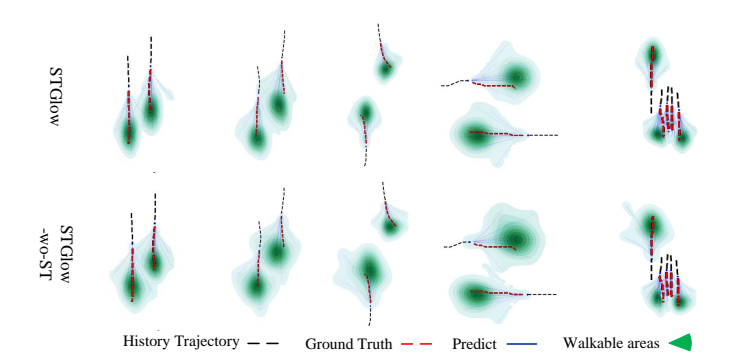


Fig. 8. Examples of diverse predictions of our method with and without dual graphormer (ST) on SDD. Black dash represents pedestrian historical trajectory, red dash denotes the ground truth trajectories, thin solid blue line represents the predicted diverse trajectories, and the green area represents the walkable area, which is visualized by the kernel density estimation map drawn from the predicted 20 trajectories. Better viewed in color.

up, making a turn, avoiding collision, and complex interactions. In these scenarios, compared to BiTraP, our method is able to make predictions that are more consistent with the laws of human motion, as we intuitively model the evolution of human motion behavior from simple to complex. For example, in the second and third rows of ETH and HOTEL, BiTraP does not handle well with slowing down and speeding up, and even predicts the future trajectory of possible collisions for parallel pedestrians, whereas our method does a good job of forecasting these challenging motion behaviors. Besides, our method adequately models temporal dependencies and the mutual spatial interactions to predict a more accurate future trajectory. For instance, in the second row of UNIV, our method can accurately forecast the making a turn behavior for parallel pedestrians in complex scenarios, while the prediction results of BiTraP in both velocity and direction show certain deviations. Similarly, in the third row, our method can accu-

TABLE III
THE ADE AND FDE PERFORMANCE OF VARIANTS ON SDD DATASET. (1)
AND (2) INDICATE GRU AND TRANSFORMER, RESPECTIVELY

	Comp	Variants			
SG	TG	PN	BiD	ADE/FDE	
✓	✓	✓		7.30/11.38	
×	(1)		\checkmark	8.80/14.75	
×	(1)	\checkmark	\checkmark	7.45/11.88	
(2)	(2)	\checkmark	\checkmark	7.33/11.56	
×	\checkmark	\checkmark	\checkmark	7.39/11.70	
\checkmark	(1)	\checkmark	\checkmark	7.53/11.84	
\checkmark	\checkmark		\checkmark	8.60/14.35	
✓	\checkmark	\checkmark	\checkmark	7.20/11.20	

rately deal with the situation of avoiding collision, because we intuitively model social interactions in both temporal and spatial domain. A similar conclusion can be drawn from the second and third rows of ZARA1 and ZARA2.

2) Results of diverse predictions: We further investigate the ability to generate diverse predictions of our method. As shown in Fig. 8, we compare the case with and without the dual graphormer. The visualization results show that our generative flow-based methods can well generate diverse and natural future trajectories in the forecast walkable area with and without social interactions. Notably, compared with the model without social interactions (as shown in the second row), our STGlow not only avoids collision to a certain extent, but also predicts a more concentrated walking area, which means that STGlow, our method that takes into account social interactions, is a better measure of the diversity and stability of forecast future trajectories.

TABLE IV
THE PERFORMANCE OF VARIANTS OF DUAL GRAPHORMER ON SDD
DATASET.

TG		Results		SG	Results		
CE	PE	A_{tmp}	ADE/FDE	SE	HE	A_{spa}	ADE/FDE
√	×	×	7.27/11.42	√	×	×	7.25/11.35
×	\checkmark	×	7.22/11.43	×	\checkmark	×	7.25/11.45
×	×	\checkmark	7.24/11.48	×	×	\checkmark	7.24/11.36
×	×	×	7.30/11.46	×	×	×	7.29/11.47
✓	✓	\checkmark	7.20/11.20	✓	\checkmark	\checkmark	7.20/11.20

F. Ablation Experiments

In this subsection, we conduct ablation experiments to investigate the effectiveness of each key component including spatial graphormer, temporal graphormer, PN in Glow, and bidirectional decoder.

- 1) Componets of our architecture: We first explore the impact of each component of our architecture, including spatial graphormer (SG), temporal graphormer (TG), pattern normalization (PN), and bidirectional decoders (BiD). In the variations of our approach, we choose GRU or Transformer to replace our TG to extract the representation of motion behaviors and use a widely-used forward decoder to replace our BiD. The ablation results are summarized in Table III. Obviously, each component in our framework provides some degree of performance improvement. Compared with the third and fifth lines, it can be seen that our TG can extract temporal dependencies better than GRU due to the considering of the temporal dependencies in both behavior-independent and behavior-dependent. Besides, considering the uniqueness of behavior pattern, our PN normalizes the behavior pattern of each pedestrian, bringing a huge performance gain compared to the last two rows. Note that our spatial and temporal graphormer is significantly better than the standard Transformer on modeling social interactions in the fourth line, which further demonstrates the effectiveness of our proposed dual graphormer. Other ablation results also demonstrated the importance of our proposed components.
- 2) Dual graphormer analysis: In order to further investigate how each component in the developed temporal graphormer (TG) and spatial graphormer (SG) impact on trajectory prediction, including the centrality encoding (CE), position embedding (PE), adjacency matrix in temporal (A_{tmp}) , spatial embedding (SE), steering embedding (HE), and adjacency matrix in spatial (A_{spa}) , corresponding ablation experiments are summarized in Table IV. As shown by the left and right groups in the table, in general, each component we designed in TG and SG facilitate the modeling of social interactions. Note that when no components are adopted, our TG and SG degenerate into commonly used Transformers, where the time step nodes and pedestrians in the scene are treated as fully connected undirected graphs. Obviously, the performance of our SG and TG is greatly improved compared to the widely used Transformer that does not consider the temporal dependencies and the mutual spatial interactions.

V. CONCLUSION

In this paper, we have introduced a novel STGlow framework for trajectory prediction. Different from previous approaches, our method can more accurately model the underlying data distribution by optimizing the exact log-likelihood of observations. Besides, our method has clear physical meanings to simulate the evolution of human motion behaviors, where the forward process of the flow gradually decouples the complex motion behavior into a series of simple behaviors, while its reverse process represents the evolution of simple behaviors to the complex motion behavior. In addition, we have designed a novel dual graphormer to extract the global social interaction of pedestrians in both temporal and spatial domains. Both quantitative and qualitative experimental results demonstrate the superiority of our approach under various situations.

REFERENCES

- J. Liang, L. Jiang, J. C. Niebles, A. G. Hauptmann, and L. Fei-Fei, "Peeking into the future: Predicting future person activities and locations in videos," in *Proc. IEEE Conf. Comput. Vis. Pattern Recogn.*, 2019, pp. 5725–5734.
- [2] P. T. Szemes, H. Hashimoto, and P. Korondi, "Pedestrian-behavior-based mobile agent control in intelligent space," *IEEE Trans. Instrum. Meas.*, vol. 54, no. 6, pp. 2250–2257, 2005.
- [3] B. Musleh, F. García, J. Otamendi, J. M. Armingol, and A. De la Escalera, "Identifying and tracking pedestrians based on sensor fusion and motion stability predictions," *Sensors*, vol. 10, no. 9, pp. 8028–8053, 2010
- [4] C. Huang, J. Wen, Y. Xu, Q. Jiang, J. Yang, Y. Wang, and D. Zhang, "Self-supervised attentive generative adversarial networks for video anomaly detection," *IEEE Trans. Neural Netw. Learn. Systems*, pp. 1–15, 2022.
- [5] V. Bastani, L. Marcenaro, and C. S. Regazzoni, "Online nonparametric bayesian activity mining and analysis from surveillance video," *IEEE Trans. Image Process.*, vol. 25, no. 5, pp. 2089–2102, 2016.
- [6] L. Lin, Y. Lu, Y. Pan, and X. Chen, "Integrating graph partitioning and matching for trajectory analysis in video surveillance," *IEEE Trans Image Process.*, vol. 21, no. 12, pp. 4844–4857, 2012.
- [7] F. Jiang, Y. Wu, and A. K. Katsaggelos, "A dynamic hierarchical clustering method for trajectory-based unusual video event detection," *IEEE Trans. Image Process.*, vol. 18, no. 4, pp. 907–913, 2009.
- [8] A. Gupta, J. Johnson, L. Fei-Fei, S. Savarese, and A. Alahi, "Social GAN: Socially acceptable trajectories with generative adversarial networks," in *Proc. IEEE Conf. Comput. Vis. Pattern Recogn.*, 2018, pp. 2255–2264
- [9] A. Mohamed, K. Qian, M. Elhoseiny, and C. Claudel, "Social-STGCNN: A social spatio-temporal graph convolutional neural network for human trajectory prediction," in *Proc. IEEE Conf. Comput. Vis. Pattern Recogn.*, 2020, pp. 14424–14432.
- [10] C. Yu, X. Ma, J. Ren, H. Zhao, and S. Yi, "Spatio-temporal graph transformer networks for pedestrian trajectory prediction," in *Proc. Eur. Conf. Comput. Vis.*, 2020, pp. 507–523.
- [11] R. Liang, Y. Li, X. Li, Y. Tang, J. Zhou, and W. Zou, "Temporal pyramid network for pedestrian trajectory prediction with multi-supervision," in *Proc. AAAI Conf. Art. Intel.*, vol. 35, 2021, pp. 2029–2037.
- [12] Y. Yuan, X. Weng, Y. Ou, and K. M. Kitani, "Agentformer: Agent-aware transformers for socio-temporal multi-agent forecasting," in *Proc. IEEE Int. Conf. Comput. Vis.*, 2021, pp. 9813–9823.
- [13] Y. Li, R. Liang, W. Wei, W. Wang, J. Zhou, and X. Li, "Temporal pyramid network with spatial-temporal attention for pedestrian trajectory prediction," *IEEE Trans. Netw. Sci. Eng.*, vol. 9, no. 3, pp. 1006–1019, 2022.
- [14] T. Gu, G. Chen, J. Li, C. Lin, Y. Rao, J. Zhou, and J. Lu, "Stochastic trajectory prediction via motion indeterminacy diffusion," in *Proc. IEEE Conf. Comput. Vis. Pattern Recogn.*, 2022, pp. 17113–17122.
- [15] H. Gao, Y. Qin, C. Hu, Y. Liu, and K. Li, "An interacting multiple model for trajectory prediction of intelligent vehicles in typical road traffic scenario," *IEEE Trans. Neural Netw. Learn. Systems*, pp. 1–12, 2021.

- [16] T. Salzmann, B. Ivanovic, P. Chakravarty, and M. Pavone, "Trajectron++: Dynamically-feasible trajectory forecasting with heterogeneous data," in *Proc. Eur. Conf. Comput. Vis.*, 2020, pp. 683–700.
- [17] I. Goodfellow, J. Pouget-Abadie, M. Mirza, B. Xu, D. Warde-Farley, S. Ozair, A. Courville, and Y. Bengio, "Generative adversarial nets," in *Proc. Adv. Neural Inf. Process. Syst.*, 2014, pp. 2672–2680.
- [18] K. Mangalam, H. Girase, S. Agarwal, K.-H. Lee, E. Adeli, J. Malik, and A. Gaidon, "It is not the journey but the destination: Endpoint conditioned trajectory prediction," in *Proc. Eur. Conf. Comput. Vis.*, 2020, pp. 759–776.
- [19] K. Mangalam, Y. An, H. Girase, and J. Malik, "From goals, waypoints & paths to long term human trajectory forecasting," in *Proc. IEEE Int. Conf. Comput. Vis.*, 2021, pp. 15233–15242.
- [20] Y. Yao, E. Atkins, M. Johnson-Roberson, R. Vasudevan, and X. Du, "Bitrap: Bi-directional pedestrian trajectory prediction with multi-modal goal estimation," *IEEE Robot. Autom. Let.*, vol. 6, no. 2, pp. 1463–1470, 2021.
- [21] G. Chen, J. Li, N. Zhou, L. Ren, and J. Lu, "Personalized trajectory prediction via distribution discrimination," in *Proc. IEEE Int. Conf. Comput. Vis.*, 2021, pp. 15580–15589.
- [22] L. Shi, L. Wang, C. Long, S. Zhou, M. Zhou, Z. Niu, and G. Hua, "Sgcn: Sparse graph convolution network for pedestrian trajectory prediction," in *Proc. IEEE Conf. Comput. Vis. Pattern Recogn.*, 2021, pp. 8994–9003.
- [23] B. Yang, G. Yan, P. Wang, C.-Y. Chan, X. Song, and Y. Chen, "A novel graph-based trajectory predictor with pseudo-oracle," *IEEE Trans. Neural Netw. Learn. Systems*, pp. 1–15, 2021.
- [24] M. Li, S. Chen, Y. Shen, G. Liu, I. W. Tsang, and Y. Zhang, "Online multi-agent forecasting with interpretable collaborative graph neural networks," *IEEE Trans. Neural Netw. Learn. Systems*, pp. 1–15, 2022.
- [25] D. Helbing and P. Molnar, "Social force model for pedestrian dynamics," Phy. rev. E, vol. 51, no. 5, pp. 4282–4286, 1995.
- [26] J. M. Wang, D. J. Fleet, and A. Hertzmann, "Gaussian process dynamical models for human motion," *IEEE Trans. Pattern Anal. Mach. Intell.*, vol. 30, no. 2, pp. 283–298, 2007.
- [27] M. K. C. Tay and C. Laugier, "Modelling smooth paths using gaussian processes," in *Proc. Field and Service Robotics*, 2008, pp. 381–390.
- [28] R. Mehran, A. Oyama, and M. Shah, "Abnormal crowd behavior detection using social force model," in *Proc. IEEE Conf. Comput. Vis. Pattern Recogn.*, 2009, pp. 935–942.
- [29] S. Pellegrini, A. Ess, K. Schindler, and L. Van Gool, "You'll never walk alone: Modeling social behavior for multi-target tracking," in *Proc. IEEE Int. Conf. Comput. Vis.*, 2009, pp. 261–268.
- [30] A. Alahi, K. Goel, V. Ramanathan, A. Robicquet, L. Fei-Fei, and S. Savarese, "Social LSTM: Human trajectory prediction in crowded spaces," in *Proc. IEEE Conf. Comput. Vis. Pattern Recogn.*, 2016, pp. 961–971.
- [31] H. Xue, D. Q. Huynh, and M. Reynolds, "Poppl: Pedestrian trajectory prediction by 1stm with automatic route class clustering," *IEEE Trans. Neural Netw. Learn. Systems*, vol. 32, no. 1, pp. 77–90, 2021.
- [32] P. Zhang, W. Ouyang, P. Zhang, J. Xue, and N. Zheng, "Sr-Istm: State refinement for lstm towards pedestrian trajectory prediction," in *Proc. IEEE Conf. Comput. Vis. Pattern Recogn.*, 2019, pp. 12085–12094.
- [33] J. Chung, K. Kastner, L. Dinh, K. Goel, A. C. Courville, and Y. Bengio, "A recurrent latent variable model for sequential data," in *Proc. Adv. Neural Inf. Process. Syst.*, 2015, pp. 2980–2988.
- [34] A. Graves and N. Jaitly, "Towards end-to-end speech recognition with recurrent neural networks," in *Proc. Int. conf. mach. learn.*, 2014, pp. 1764–1772.
- [35] O. Vinyals, A. Toshev, S. Bengio, and D. Erhan, "Show and tell: A neural image caption generator," in *Proc. IEEE Conf. Comput. Vis. Pattern Recogn.*, 2015, pp. 3156–3164.
- [36] Y. Hu, S. Chen, Y. Zhang, and X. Gu, "Collaborative motion prediction via neural motion message passing," in *Proc. IEEE Conf. Comput. Vis. Pattern Recogn.*, 2020, pp. 6319–6328.
- [37] Y. Xu, J. Yang, and S. Du, "Cf-lstm: cascaded feature-based long short-term networks for predicting pedestrian trajectory," in *Proc. AAAI Conf. Art. Intel.*, vol. 34, no. 07, 2020, pp. 12541–12548.
- [38] A. Vemula, K. Muelling, and J. Oh, "Social attention: Modeling attention in human crowds," in *Proc. IEEE int. Conf. Robot. and Auto.*, 2018, pp. 1–7.
- [39] Y. Huang, H. Bi, Z. Li, T. Mao, and Z. Wang, "STGAT: Modeling spatial-temporal interactions for human trajectory prediction," in *Proc.* IEEE Int. Conf. Comput. Vis., 2019, pp. 6272–6281.
- [40] I. Bae and H.-G. Jeon, "Disentangled multi-relational graph convolutional network for pedestrian trajectory prediction," in *Proc. AAAI Conf. Art. Intel.*, vol. 35, 2021, pp. 911–919.

- [41] C. Ying, T. Cai, S. Luo, S. Zheng, G. Ke, D. He, Y. Shen, and T.-Y. Liu, "Do transformers really perform badly for graph representation?" in *Proc. Adv. Neu. Inf. Process. Syst.*, vol. 34, 2021, pp. 28877–28888.
- [42] T. Zhao, Y. Xu, M. Monfort, W. Choi, C. Baker, Y. Zhao, Y. Wang, and Y. N. Wu, "Multi-agent tensor fusion for contextual trajectory prediction," in *Proc. IEEE Conf. Comput. Vis. Pattern Recogn.*, 2019, pp. 12126–12134.
- [43] J. Li, H. Ma, and M. Tomizuka, "Conditional generative neural system for probabilistic trajectory prediction," in *Proc. IEEE Int. Conf. Intel. Robots and Sys.*, 2019.
- [44] L. Dinh, D. Krueger, and Y. Bengio, "Nice: Non-linear independent components estimation," arXiv preprint arXiv:1410.8516, 2014.
- [45] L. Dinh, J. Sohl-Dickstein, and S. Bengio, "Density estimation using real nvp," arXiv preprint arXiv:1605.08803, 2016.
- [46] D. P. Kingma and P. Dhariwal, "Glow: Generative flow with invertible 1x1 convolutions," in *Proc. Adv. Neu. Inf. Process. Syst.*, vol. 31, 2018, pp. 10236–10245.
- [47] A. Lugmayr, M. Danelljan, L. V. Gool, and R. Timofte, "Srflow: Learning the super-resolution space with normalizing flow," in *Proc. Eur. Conf. Comput. Vis.*, 2020, pp. 715–732.
- [48] M. Kumar, M. Babaeizadeh, D. Erhan, C. Finn, S. Levine, L. Dinh, and D. Kingma, "Videoflow: A flow-based generative model for video," arXiv preprint arXiv:1903.01434, 2019.
- [49] R. Prenger, R. Valle, and B. Catanzaro, "Waveglow: A flow-based generative network for speech synthesis," in *IEEE Int. Conf. Acoust. Speech Signal Process.*, 2019, pp. 3617–3621.
- [50] S. Kim, S.-g. Lee, J. Song, J. Kim, and S. Yoon, "Flowavenet: A generative flow for raw audio," arXiv preprint arXiv:1811.02155, 2018.
- [51] A. Vaswani, N. Shazeer, N. Parmar, J. Uszkoreit, L. Jones, A. N. Gomez, Ł. Kaiser, and I. Polosukhin, "Attention is all you need," in *Proc. Adv. Neural Inf. Process. Syst.*, 2017, pp. 5998–6008.
- [52] J. Devlin, M.-W. Chang, K. Lee, and K. Toutanova, "Bert: Pre-training of deep bidirectional transformers for language understanding," arXiv preprint arXiv:1810.04805, 2018.
- [53] T. Brown, B. Mann, N. Ryder, M. Subbiah, J. D. Kaplan, P. Dhariwal, A. Neelakantan, P. Shyam, G. Sastry, A. Askell et al., "Language models are few-shot learners," Advances in neural information processing systems, vol. 33, pp. 1877–1901, 2020.
- [54] A. Dosovitskiy, L. Beyer, A. Kolesnikov, D. Weissenborn, X. Zhai, T. Unterthiner, M. Dehghani, M. Minderer, G. Heigold, S. Gelly et al., "An image is worth 16x16 words: Transformers for image recognition at scale," arXiv preprint arXiv:2010.11929, 2020.
- [55] K. Han, A. Xiao, E. Wu, J. Guo, C. Xu, and Y. Wang, "Transformer in transformer," Advances in Neural Information Processing Systems, vol. 34, pp. 15 908–15 919, 2021.
- [56] L. Yuan, Y. Chen, T. Wang, W. Yu, Y. Shi, Z.-H. Jiang, F. E. Tay, J. Feng, and S. Yan, "Tokens-to-token vit: Training vision transformers from scratch on imagenet," in *Proc. IEEE Int. Conf. Comput. Vis.*, 2021, pp. 558–567.
- [57] J. You, Y. Li, J. Zhou, Z. Hua, W. Sun, and X. Li, "A transformer based approach for image manipulation chain detection," in *Proc. ACM Int. Conf. Multi.*, 2021, pp. 3510–3517.
- [58] Q. Song, B. Sun, and S. Li, "Multimodal sparse transformer network for audio-visual speech recognition," *IEEE Trans. Neural Netw. Learn. Systems*, pp. 1–11, 2022.
- [59] X. Zhu, W. Su, L. Lu, B. Li, X. Wang, and J. Dai, "Deformable detr: Deformable transformers for end-to-end object detection," arXiv preprint arXiv:2010.04159, 2020.
- [60] J. L. Ba, J. R. Kiros, and G. E. Hinton, "Layer normalization," arXiv preprint arXiv:1607.06450, 2016.
- [61] J. Duan, L. Wang, C. Long, S. Zhou, F. Zheng, L. Shi, and G. Hua, "Complementary attention gated network for pedestrian trajectory prediction," in *Proc. AAAI Conf. Art. Intel.*, 2022.
- [62] D. P. Kingma and J. Ba, "Adam: A method for stochastic optimization," arXiv preprint arXiv:1412.6980, 2014.
- [63] A. Lerner, Y. Chrysanthou, and D. Lischinski, "Crowds by example," Computer graphics forum, vol. 26, no. 3, pp. 655–664, 2007.
- [64] A. Robicquet, A. Sadeghian, A. Alahi, and S. Savarese, "Learning social etiquette: Human trajectory understanding in crowded scenes," in *Proc. Eur. Conf. Comput. Vis.*, 2016, pp. 549–565.
- [65] L. Shi, L. Wang, C. Long, S. Zhou, F. Zheng, N. Zheng, and G. Hua, "Social interpretable tree for pedestrian trajectory prediction," arXiv preprint arXiv:2205.13296, 2022.